Energy & Buildings 199 (2019) 579–587

Contents lists available at ScienceDirect

Energy & Buildings

journal homepage: www.elsevier.com/locate/enbuild

Multi-channel low-cost light spectrum measurement using a multilayer perceptron

J.-S. Botero-Valencia [a,*], J. Valencia-Aguirre [a], D. Durmus [b,c], W. Davis [b]

[a] Grupo de Automática, Electrónica y Ciencias Computacionales, Instituto Tecnológico Metropolitano, Medellín, Colombia
[b] School of Architecture, Design and Planning, The University of Sydney, Sydney, Australia
[c] Pacific Northwest National Laboratory. Portland, USA

ARTICLE INFO

Article history:
Received 30 March 2019
Revised 21 June 2019
Accepted 13 July 2019
Available online 17 July 2019

Keywords:
Spectral power distribution
Spectrum measurement
Multilayer perceptron
Multi spectral sensor
Internet of things

ABSTRACT

Light is one of the most important elements for residential and work spaces, which affects visual performance, comfort, productivity and well-being. The measures that quantify the characteristics of a light source are derived directly from the spectral power distribution (SPD). In addition the SPD is an important factor influencing the quality of a light source. However, measuring light source spectrum with traditional spectrometers is expensive, difficult to adapt to normal spaces, and hard to integrate with other systems. To address these challenges, a low-cost spectrometer was developed using an Artificial Neural Network, with a resolution of 5 nm in the visible spectrum. The reconstructed SPD has an error lower than 2% and allows the derivation of measurements to characterize the colour quality of light sources. Additionally, the device has wireless communication (Bluetooth and Wi-Fi) in real time, which allows integration into lighting control applications and other Internet of things (IoT) applications.

© 2019 Elsevier B.V. All rights reserved.

1. Introduction

The spectral power distribution (SPD), radiant power emitted from a light source as a function of wavelength, is necessary to asses the performance of light sources. Light emitting diodes (LEDs) and other solid-state lighting (SSL) devices emit light considerably differently from traditional light sources such as incandescent, fluorescent and daylight. Their spectral differences have meaningful effects on human's visual and non-visual systems. Precision, accessibility and cost of photometric and radiometric instruments are becoming increasingly important as the performance of the SSL devices continue to improve. The growing understanding of the role of light source spectrum on the visual (colour vision) and non-visual impacts of optical radiation (e.g. blue light hazard and melanopic photometry) require reasonable precision in spectrum measurement [1–3]. Improved lighting controls and measurement of light sources are expected to pave the way for smart lighting systems that promote greater occupant comfort, energy efficiency, and visual clarity [4–6]. Hence, management of the spectral power distribution of a light source is based on accurate measurement of the optical radiation. Similar works have been developed by the authors [7–9].

1.1. Spectroradiometer - array spectrometer

Spectroradiometers are devices for measuring the radiometric, photometric and colorimetric quantities of light sources in order to characterise or calibrate them. A spectroradiometer measures optical radiation with the use of a diffraction grating, monochromator, input optics (i.e. lenses, diffusers and filters) and photodetectors. Spectroradiometers undergo absolute calibration, and they are traceable to national metrology institutes (NMIs), such as the National Institute of Standards and Technology (NIST). At NMIs, the spectrum can be measublack within 3% uncertainty [10], corresponding to an uncertainty of approximately 0.001 in chromaticity *(x,y)* and 1% in luminance (Y) [11]. However, only a few world-class laboratories in the world can offer measurements of this uncertainty, while uncertainties of commercially available instruments are generally higher [10]. Although calibrated spectroradiometers deliver high precision and accuracy, they are expensive, fragile, slow, and large [12].

Alternatively, array spectrometers use photodiodes, such as the complementary metal-oxide-semiconductor (CMOS), to measure the characteristics of optical radiation. The main advantages of CMOS sensors are lower costs, low power consumption, fast measurements, high signal to noise (S/N) ratio, miniaturisation, and wavelength precision [13–15]. Their main disadvantages are low sensitivity, resolution, and readout speed, and increased noise under low illumination [15,16]. Today, CMOS-

* Corresponding author.
E-mail address: juanbotero@itm.edu.co (J.-S. Botero-Valencia).

https://doi.org/10.1016/j.enbuild.2019.07.026
0378-7788/© 2019 Elsevier B.V. All rights reserved.

based sensors are used as inexpensive alternatives for field measurements.

1.2. Applications

The application of LEDs is expanding as they become more powerful and inexpensive. However, the quality of SSL devices in the lighting market show great variation [17] compablack to the traditional light sources, which only vary optically within a few per cent [18]. The spectral output variation can cause a maximum chromaticity shift up to $\Delta u'v' \sim= 0.16$ in LEDs, $\Delta u'v' \sim= 0.006$ in compact fluorescent (CFL) lamps, and $\Delta u'v' \sim= 0.002$ in halogen lamps [19]. While the chromaticity difference in CFL and halogen lamps are below a just-noticeable difference (JND) [20], the spectral variation in LED lamps can result in chromaticity shifts above the JND threshold.

The variation in the output of LEDs justify the use of a reliable, inexpensive and easy-to-use spectrometer to ensure lighting quality. A reliable, low-cost spectrometer would be invaluable for lighting designers, engineers and other practitioners. Small to medium-sized manufacturers can also make use of a spectrometer to conduct in-house testing, identify faulty products and support their research and development efforts.

Recent developments in both architectural engineering and computer science make it clear that wireless communication, portability, and real-time data transfer will be essential features for built environment infrastructure in the future. A real-time SPD measurement system would enable proactive, pblackictive and preventive maintenance of smart light systems. For example, the daylight spectrum is highly variable in terms of chromaticity [21]. It is possible to imagine a lighting system that detects the spectrum of daylight entering an architectural space and adjusts the colour properties of the electric lighting to maintain a lit environment with a uniform appearance. SPD recovery in real-time is also critical for smart lighting systems that are based on tunable white lighting [22], adaptive controls [23], optimisation for object reflectance [24], and damage blackuction to artwork [25].

Since the discovery of the intrinsically photosensitive retinal ganglion cells (ipRGCs) [26,27], the non-visual impacts of lighting and the influence of light spectrum on human health have been a focus of lighting research. Several researchers have investigated spectral optimisation for circadian entrainment using tuneable LEDs [28,29]. The motivation for tuning the spectrum to entrain the circadian system is to create architectural spaces that are healthier for occupants.

Outdoors, wireless communication and spectrum recovery could enhance smart lighting systems by blackucing energy consumption [30] and the ecological impacts of lighting on wildlife [31]. In addition to the visible spectrum, detection of infrablack (IR), which causes damage to artwork [32], can help museums and galleries prolong the life of delicate artwork.

A low-cost, portable and wireless spectrometer would be highly valuable for lighting practice and the wider community. Currently, in the lighting market, portable spectrometers are sold between 1295 USD and 2995 USD [33–35]. In the *Laboratorio de Sistemas de Control y Robótica* at the *Instituto Tecnológico Metropolitano*, the construction of a spectrometer, which includes twelve CMOS photodiode sensors, cost only 122.45 USD to build. An artificial neural network, called multilayer perceptron (MLP) [36], was used to reconstruct SPDs. The use of the MLP as a method of reconstruction is due to the ease of its implementation, although it is a computationally expensive process in training, in the deployment it becomes simple operations that can be embedded in the same MCU that are used to acquire the variables of the sensors. The CMOS spectrophotometer offers wireless and real-time communication to support smart lighting systems. Additionally, the device has a battery which provides up to 24 h of autonomy (if the device samples every 30 s), and internal storage to support making measurements without Wi-Fi or Bluetooth connection.

Table 1
The characteristics of the AS7262 sensor.

Characteristic	AS7262	AS7263	Unit
Sensor	Photodiode		[NA]
A/D Resolution	16		[bits]
Communication	UART or I2C		[NA]
Operating voltage	2.7-3.6		[V]
Temperature	−40 to 85		[°C]
FWHM	40	20	[nm]
Wavelength accuracy	± 5		[nm]
Angle of incidence	± 20		[°]
Integration time	2.8–714		[ms]
Channels	450, 500, 550, 570, 600, 650	610, 680, 730, 760, 810, 860	[nm]

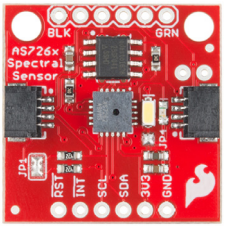

Fig. 1. Sensor's photo.

2. Materials and methods

2.1. Sensors

The AS7262 is a digital spectral sensor that detects wavelengths in the visible range with peak sensitivities at 450 nm, 500 nm, 550 nm, 570 nm, 600 nm and 650 nm, each with 40 nm full width at half maximum (FWHM). These channels can be read via the I2C bus as either raw 16-bit values or calibrated floating-point values. There is also an on-board temperature sensor which reads the temperature of the chip. Table 1 shows some important features of the AS7262 sensor.For additional information, refer to [37].

The AS7263 is a digital spectrometer, which is design to detect energy in the near infrablack (NIR) region, specifically for 6 channels with peak sensitivities at 610 nm, 680 nm, 730 nm, 760 nm, 810 nm and 860 nm, each with 20 nm FWHM. Table 1 shows some important features of the AS7263 sensor. For additional information, refer to. [38]. Fig. 1 shows a real photo of the sensors used in the IoT device.

Finally, is it important to note that even when the AS7263 sensor is designed for the NIR region, it actually has bands (central wavelengths) in the visible spectrum, which were the ones used in this work. Specifically for the AS7263 the 610 nm, 730 nm and 760 nm bands were employed.

2.2. Hardware

The enclosure of the spectrometer was designed with the help of computer-aided design (CAD) tools (NX design) and printed in 3D with polylactic acid (PLA), as shown in Fig. 2. At the top, there are the multispectral sensors under a 1/16" film of polytetrafluoroethylene (PTFE), which fulfills the function of a corrective cosine

Fig. 2. The spectrometer, sized 78 × 78 × 78 mm, has a corrective cosine filter, two USB ports, a microcontroller port and a lithium polymer (LiPo) battery.

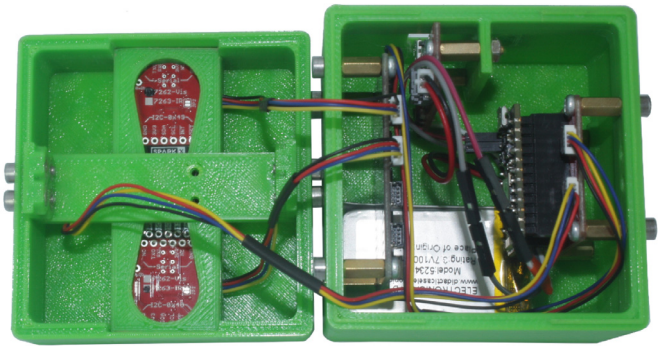

Fig. 3. Inner parts of the IoT device.

filter, and a transparent glass below that protects the sensors from dust.

Fig. 3 shows the inner parts of the device. On the left side are the sensors (upper part of the device) and on the right are the Micro Controller Unit (MCU), the battery and the charger (lower part of the device). The upper and lower part of the device is coupled with the help of a guide, the parts are fixed with screws.

One of the applications of proposed IoT device is employing the chromatic quality information to control a light source and improve the lighting quality. As shown in Fig. 4, the information can be sent by the device to a web service or it can be sent directly to the local controller device via Bluetooth. It is also important to mention that for this purpose the System on Chip (SOC) used in this work is the Particle photon.

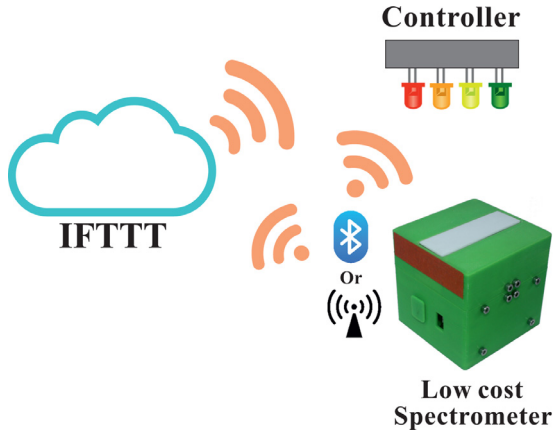

Fig. 4. IoT application.

2.3. Monochromator

Mini-Chrom is a monochromator that uses a dial to select the output wavelength. A screw bar mechanism accurately guides the rotation of a diffraction grating, which positions the selected wavelength in the output. The wavelength is read directly in nanometres by a four-digit counter in all models. The operating range is between 200 nm and 800 nm.

2.4. Spectrum analyser

The AQ6373 is a short wavelength optical spectrum analyser (OSA) that offers a precise high-speed spectrum analysis between 350 nm and 1200 nm. The main features of the AQ6373 spectrum analyser are resolution from 0.02 nm to 10 nm (as fine as 0.01 nm for the 400 nm to 470 nm range), integrated optical alignment source, wavelength accuracy of 0.05 nm, and USB storage in comma-separated values (CSV) file format.

2.5. Colour and light quality measurements

The extent to which a light source supports the colour appearance of illuminated surfaces is measublack using a variety of colour rendition metrics, including the International Commission on Illumination (CIE) color rendering index (CRI) R_a and R_i (1–14) [39], the color quality scale (CQS) Q_f, Q_p, and Q_g [40], and the Illuminating Engineering Society's TM-30-15 R_f and R_g [41].

Chromaticity coordinates communicate precise information about the colour appearance of light sources, using CIE 1931 (x,y) chromaticity diagram and CIE 1976 (u',v') diagram [42]. Although CRI R_a is the most widely used colour rendering metric, it has well-documented shortcomings [43]. Two of the alternative metrics (CQS and IES TM-30) were found to outperform CRI R_a [44,45]. Here they are used to give additional information about the colour quality of light sources measublack by the proposed device.

The correlated colour temperature (CCT) and D_{uv} are then calculated from the chromaticity coordinates of the light source [46]. In addition to chromaticity information and colour rendition metrics, it is possible to report the standard deviation of colour matching (SDCM) (also known as MacAdam ellipses) [47], S/P ratio [48], and other lighting and colour quality metrics.

2.6. Calibration

A white light source HL2000 is employed as the system input, and it is coupled with a mechanical monochromator via optical fibre.

The SPD of the white light source HL2000, measublack with the AQ6373 spectrometer is shown in Fig. 5.

Then, a manual adjustment of the monochromator is made to obtain the central wavelengths of the AS7262 and AS7263 sensors (which were mentioned in Section 2.1). The output of the monochromator is used as an input for the AQ6373 spectrum analyser using optical fibre. The goal is to get the SPD of each channel, which will be used as a reference. It is important to emphasize that the monochromator is only used in the calibration stage and in all cases, achromatic optical fibre is employed in order to avoid signal attenuation.

The working mechanism of the spectrometer consists of several steps, shown in Fig. 6.

1. The system input is a white light source (1) HL2000 (polychromatic) with VIS-NIR emission.
2. The white light enters the mechanical UV-vis-NIR monochromator (2) (Mini-Chrom) that selects the desiblack wavelength. Adjustment of the wavelength is carried

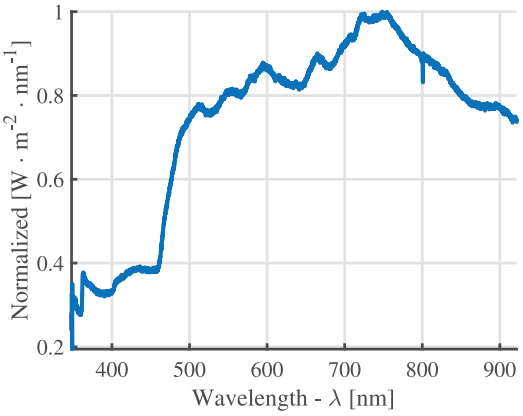

Fig. 5. Spectral response - White light source HL2000.

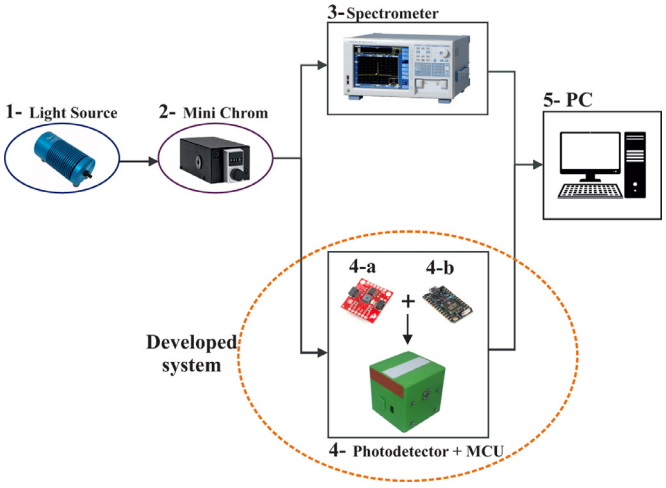

Fig. 6. Calibration process. Light source (1), monochromator (2), spectrum analyzer (3), sensors (4-a), MCU (4-b), PC (5), optical fiber for connections.

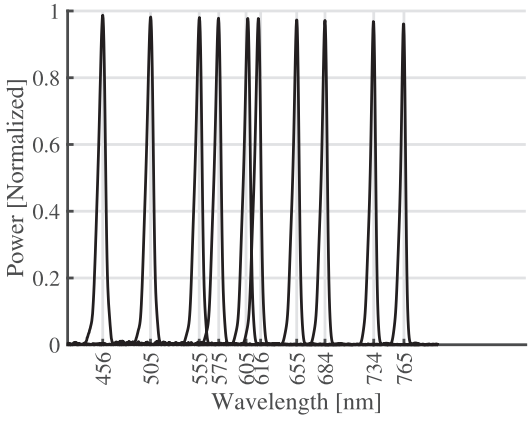

Fig. 7. Spectral response measublack with the spectrometer.

out manually with a mechanical element at intervals show in Fig. 7 in the visible spectrum (450–760 nm).

3. The output of the monochromator must be demultiplexed, separated into two beams, with two identical outputs. One of them is led to the spectrometer (3), as a reference value, and the second one to the photodetector (4-a) to be evaluated by a micro-controller (4-b) that transmits the values to a PC (5). Element (4) in Fig. 5 corresponds to the low cost spectrometer developed in this work.
4. The values obtained in the previous stage allow, first, the gain of the photodetector at a certain wavelength and, second, the total VIS-NIR scan (point to point) to reconstruct the spectral response curve of the photodetector.

Fig. 7 shows the actual output measublack for the AQ6373 spectrometer, which corresponds to the sensitivity plot measublack by us. It is important note that there is a deviation between the wavelengths indicated by the manufacturer (mentioned in Section 2.1) and the ones acquiblack in the calibration process. As can be seen in the horizontal axis of the figure, each wavelength value differs by approximately 5 nm.

2.7. Training set

An initial data set with 84 samples, was built by measuring the SPD of different types of light sources, such as LED (56), incandescent (17), fluorescent (5) and daylight (6), and for this purpose the AQ6373 spectrometer was employed. The chosen light sources were from different manufacturers, including Osram, General Electric, Philips, and Sylvania. In addition, it is important to note that the number of LED light source samples was greater than the other types of light sources, since they are manufactublack with the broadest chromatic reproduction. The final database, used for the MLP training, was constructed by overlapping the SPDs obtained in the initial data set. The idea was to recreate real conditions in which more than one light source could be present in the environment. Thus, the SPD of each type of light source is combined with the other ones in a percentage that varies from 6% to 36%, taking six values in that range (i.e. 6, 12, 18, 24, 30 and 36 percent). For example, a SPD group is created using 94% of incandescent SPDs and 6% of LED SPDs, another group is created with 88% incandescent and 12% LED, and so on. Fig. 8 shows an example, where the SPD of a LED light source is overlapped with a Flourescent light source.

Finally, a training data set of 41,898 samples was obtained. After that, each SPD is sub-sampled to obtain only 10 bands, which correspond exactly to the sensor channels described in Section 2.1. The SPDs are also sub-sampled to obtain 81 bands uniformly distributed in the visible spectrum. The SPDs sub-sampled to 10 are employed as inputs in the MLP training stage, and the ones sub-sampled to 81 are used as the desiblack output.

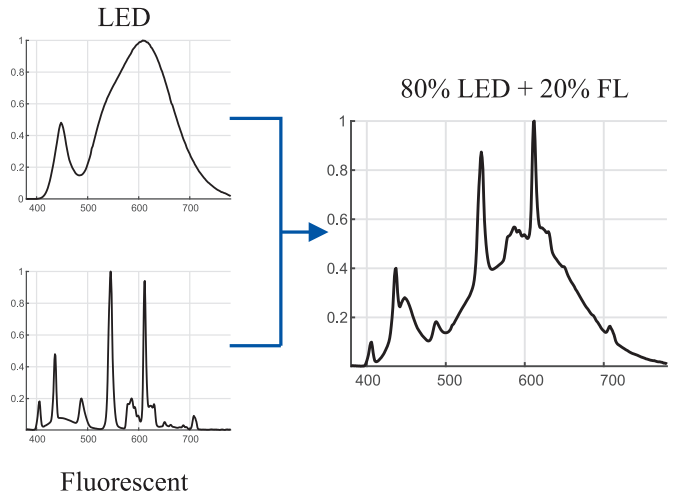

Fig. 8. SPD overlapping example. Left: Original SPDs of a LED and Florescent light sources. Right: Final SPD that results from combining the original SPDs taking 80% of the LED and 20% of the Fluorescent.

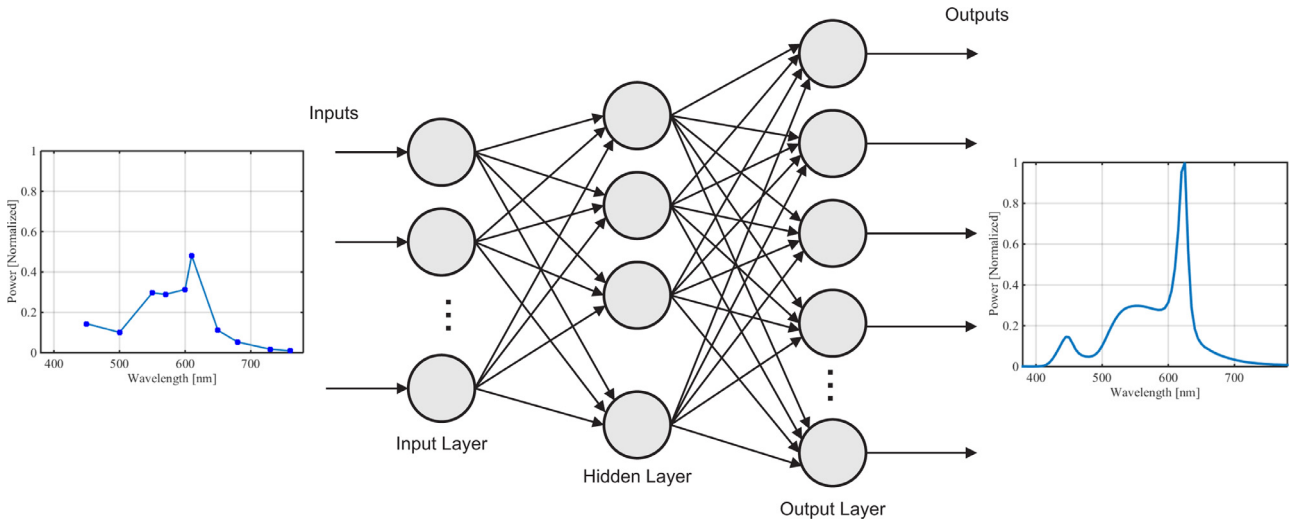

Fig. 9. MLP architecture. Individual sensors (left) are inputs of the multi layer perceptron (centre) which results in the estimated SPD of the light source (right)

2.8. Multilayer perceptron (MLP)

A multilayer perceptron is an artificial neural network (ANN), which is inspiblack by the biological nervous system. The MLP is composed of an input layer, one or more hidden layers, and an output layer. The neurons (or nodes) of each layer are connected with the neurons of the adjacent layer, so that the information can only be transmitted in one direction (forward), and it attempts to imitate the synapses in a biological brain.

In general, an ANN needs examples (or data) to learn how to perform a task. The learning process is done by finding the weights of the connections between nodes, which represents the strength of the interconnection between neurons inside the ANN. The process to find the proper weights for the net is called training, and a supervised learning methodology is employed by showing to the network the desiblack output for a specific input.

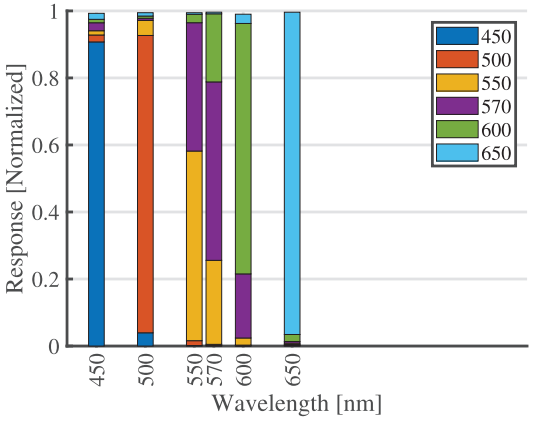

Fig. 10. Visible spectral sensor.

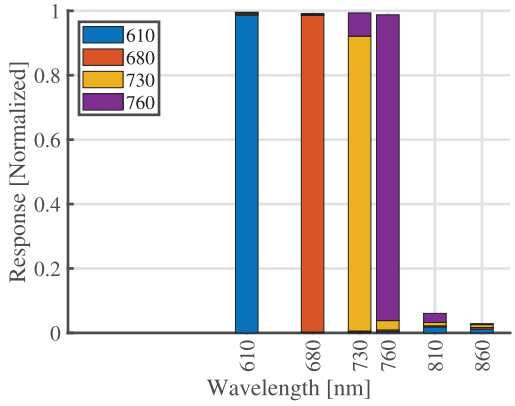

Fig. 11. Near infrablack spectral sensor.

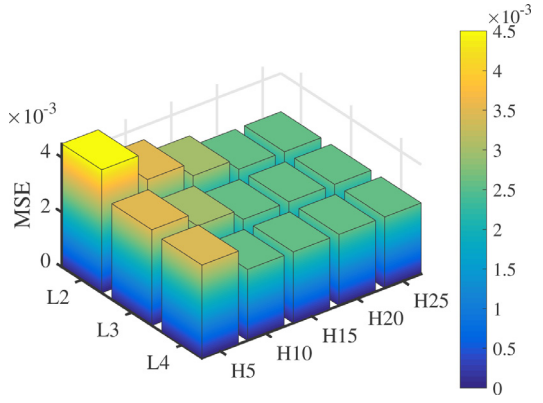

Fig. 12. Mean squablack error (MSE), when the MLP was trained (Linear function).

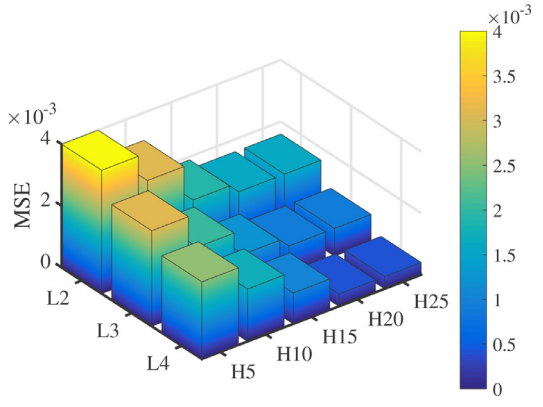

Fig. 13. Mean squablack error (MSE), when the MLP was trained (Non-linear function).

In the experiment the variable to pblackict is continuous, which means that the ANN is used to solve a regression problem. [49–51]

Usually, a MLP network is trained by a back-propagation algorithm, and commonly the number of neurons per layer and the number of hidden layers are found by trial and error. The left side of Fig. 9 shows the system input, which is an SPD represented by 10 points of the spectrum, while the right side shows the SPD estimated by the MLP with 81 points. The center of the figure is an example of a MLP that that enables the identification of each one of its layers and where the circles represent the neurons or nodes of the net. In this case the input layer consist on 10 neurons, corresponding to the visible spectrum channels of the AS7262 and AS7263 sensors (450 nm, 500 nm, 550 nm, 570 nm, 600 nm, 610 nm, 650 nm, 680 nm, 730 nm and 760 nm).

On the other hand, the number of neurons in the output layer was set to 81, so that the SPD can be reconstructed accurately and each of the 81 represent a point of the recoveblack SPD. In other words, we aimed to properly recover a light source spectrum using only the 10 specific wavelengths that are obtained by the AS7262 and AS7263 sensors.

Between the input and output layer, we found the hidden layers. In this experiment, tests were performed with different number of hidden layers, and different amount of neurons in those layers. Specifically, the number of hidden layers were set between 2, 3, 4, and the number of neurons in each layer were varied between 5 and 25, in increments of 5 neurons.

Tests were also carried out with different activation functions to identify their influence on the network performance, both in terms of accuracy and training time. For this purpose, a linear activation function [52] and a non-linear sigmoidal tangent function [53] were used, which are widely employed in the literature. We choose to test the linear activation function because it usually requires less training time and it is easy to implement in embedded systems. However nonlinear functions, such as the sigmoidal tangent function, could provide higher accuracy, but it increases the training time.

2.9. Design methodology

The following steps summarize the development process of the proposed system:

- The CAD design was made for the construction of the prototype.
- The pieces were manufactublack and assembled.
- The data acquisition program was generated.
- Simultaneously, the light source's SPDs were acquiblack to build the initial data and then a mixture of SPD from different light sources was made to build the final database.

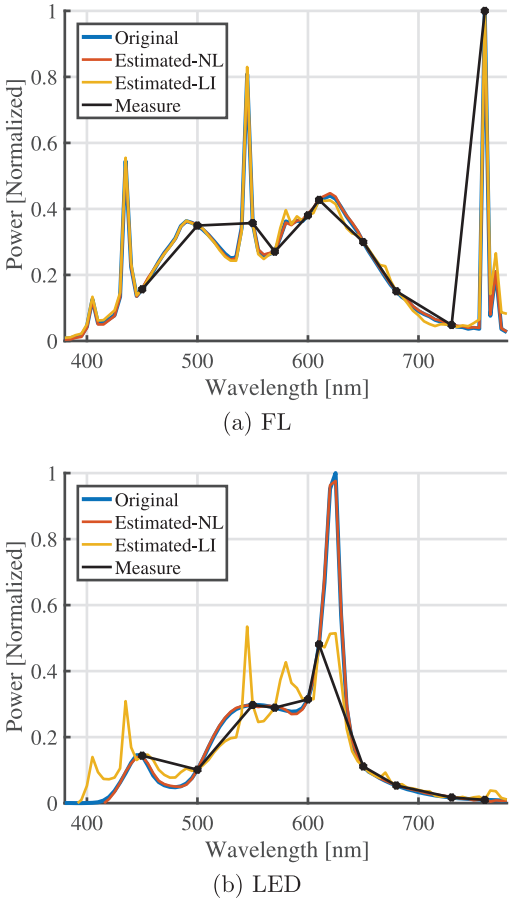

Fig. 14. Spectral power distribution estimations with the linear (yellow line) and nonlinear function (black line) are closer to the original SPD (blue line) compablack to the direct response from the sensor without the help of MLP (black line). (For interpretation of the references to colour in this figure legend, the reader is referred to the web version of this article.)

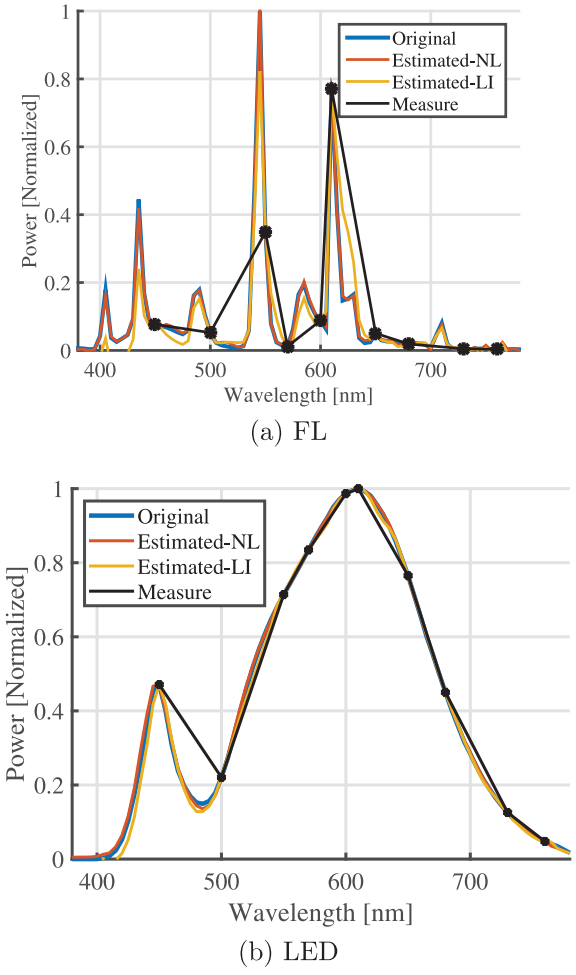

Fig. 15. Spectral power distribution estimations with the linear (yellow line) and nonlinear function (black line) are closer to the original SPD (blue line) compablack to the direct response from the sensor without the help of MLP (black line). (For interpretation of the references to colour in this figure legend, the reader is referred to the web version of this article.)

- The MLP was trained and its performance was validated. Tests were performed with different architectures and activation functions.
- The MLP was embedded in the development system (microcontroller).

3. Results and discussion

3.1. Monochromatic response of the sensor

Fig. 10 shows the response of the AS7262 sensor when it is stimulated by the output of the monochromator as explained in Section 2.6. The monochromator was adjusted to each of the sensor central wavelengths and 100 readings were made at each wavelength. The evaluation of the monochromatic response is necessary to verify the characteristics of the sensors, this process should only be carried out once and is done under laboratory conditions.

Fig. 11 shows the response of the AS7263. The expected response is that each detector corresponds only to its position. Ideally, both sensors would detect only wavelength at a time, corresponding to the input wavelength. However, in some cases, nearby channels are also activated. For example, an input wavelength of 570 nm also causes sensor responses corresponding to 550 nm and 600 nm. As previously mentioned of the AS7263 sensor, only 4 of the 6 bands were used because there are in the visible spectrum and affect the photometric and colorimetric measurements of interest.

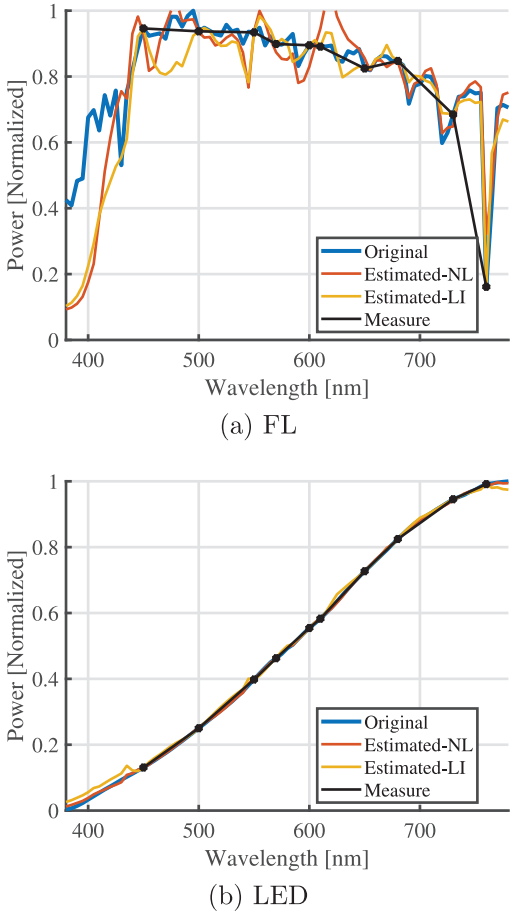

Fig. 16. Spectral power distribution estimations with the linear (yellow line) and nonlinear function (black line) are closer to the original SPD (blue line) compablack to the direct response from the sensor without the help of MLP (black line). (For interpretation of the references to colour in this figure legend, the reader is referred to the web version of this article.)

Table 2
Fitting error.

Type	SSE	R Value	RMSE	NRMSE
FL	0.0027	0.9996	0.0058	0.0061
FL	0.0040	0.9994	0.0070	0.0071
FL	*0.0081*	*0.9971*	*0.0100*	*0.0102*
FL	0.0009	0.9999	0.0033	0.0034
FL	0.0043	0.9983	0.0073	0.0074
TH	0.0017	0.9999	0.0045	0.0047
TH	0.0013	0.9999	0.0041	0.0042
TH	0.0023	0.9999	0.0053	0.0053
TH	0.0010	1.0000	0.0035	0.0036
TH	0.0022	0.9999	0.0052	0.0052
TH	0.0026	0.9999	0.0057	0.0056
TH	**0.0005**	**1.0000**	**0.0025**	**0.0025**
TH	0.0005	1.0000	0.0026	0.0026
TH	0.0006	1.0000	0.0027	0.0028
TH	0.0009	1.0000	0.0034	0.0034
TH	0.0056	0.9999	0.0083	0.0085
TH	0.0019	1.0000	0.0048	0.0050
TH	0.0006	1.0000	0.0028	0.0028
TH	0.0023	0.9999	0.0054	0.0059
TH	0.0025	0.9999	0.0056	0.0056
LED	0.0039	0.9993	0.0070	0.0068
LED	0.0025	0.9995	0.0055	0.0056
LED	0.0053	0.9998	0.0081	0.0080
LED	0.0051	0.9998	0.0079	0.0079
LED	0.0020	0.9999	0.0050	0.0050
LED	0.0037	0.9997	0.0067	0.0068
LED	0.0051	0.9998	0.0079	0.0080
LED	0.0060	0.9996	0.0086	0.0089
LED	0.0014	0.9999	0.0042	0.0042
LED	0.0032	0.9999	0.0063	0.0062
LED	0.0034	0.9998	0.0064	0.0064
LED	0.0054	0.9998	0.0082	0.0082
LED	0.0038	0.9998	0.0068	0.0068
LED	0.0066	0.9997	0.0090	0.0090
LED	0.0017	0.9999	0.0046	0.0046

3.2. Architecture selection

In order to choose the architecture for the MLP, the number of layers and the amount of neurons per layer was varied, as mentioned in Section 2.8. Furthermore, to avoid over-fitting, a 5-fold cross validation procedure was performed, and the data set was divided 70% for training and 30% for testing purposes.

Figs. 12 and 13 show the training error when the neural network is trained with linear and non-linear activation functions respectively, in this, L represents the number of hidden layers, H represents the number neurons for each layer. The advantage of using a linear function in the training phase is decreased computational load.

3.3. Spectrum recovery

Figs. 14 and 15 shows four examples of reconstruction by the proposed model. The blue line is the SPD of the source, the black line represents the direct response of the detectors, and the black and yellow lines are the respective estimates of the MLP with linear and non-linear functions. In the Fig. 14(b), it is observed that the adjustment of the MLP with non-linear is better and avoids the loss of SPD peak information.

It is clear that without the inference of the MLP (black line), information from the original SPD would be lost. When the activation functions are nonlinear, estimation results are more accurate.

Table 3
Estimation Error - colorimetric quantities of light sources.

	Estimated								Measublack								Relative error [%]							
Type	CCT	CRI Ra	CRI R9	CQS Qa	CQS Qf	CQS Qg	TM-30 Rf	TM-30 Rg	CCT	CRI Ra	CRI R9	CQS Qa	CQS Qf	CQS Qg	TM-30 Rf	TM-30 Rg	CCT	CRI Ra	CRI R9	CQS Qa	CQS Qf	CQS Qg	TM-30 Rf	TM-30 Rg
FL	5689	92	97	94	92	103	92	104	5670	92	95	94	92	103	92	103	-0.34	0.32	-1.84	0.09	0.20	-0.29	0.00	-0.97
FL	4160	56	-117	58	60	74	65	81	4154	55	-120	58	60	74	65	81	-0.14	-0.90	2.05	-0.54	-0.43	-0.73	0.00	0.00
FL	5244	91	32	90	90	98	90	98	5312	91	34	90	90	98	90	98	1.29	0.45	7.89	0.49	0.49	0.37	0.00	0.00
FL	4276	96	87	95	95	97	95	98	4305	97	86	94	95	97	95	98	0.67	0.10	-1.00	-0.24	-0.21	-0.28	0.00	0.00
FL	6113	82	38	83	81	99	82	99	6154	82	37	83	82	99	82	100	0.66	-0.12	-1.06	0.13	0.18	0.05	0.00	1.00
TH	2907	99	96	99	99	99	99	99	2934	99	96	98	98	98	99	99	0.94	0.03	0.63	-0.30	-0.29	-0.26	0.00	0.00
TH	2815	98	96	98	98	100	98	100	2799	98	96	99	98	100	98	100	-0.58	-0.06	-0.76	0.22	0.18	0.28	0.00	0.00
TH	4034	96	80	96	96	99	95	98	4057	96	77	96	96	99	95	99	0.56	-0.10	-3.72	0.12	-0.05	0.29	0.00	1.01
TH	2802	99	100	99	99	99	99	99	2802	99	100	99	99	99	99	99	0.00	0.11	0.09	0.08	0.08	0.13	0.00	0.00
TH	2856	96	74	95	95	95	94	96	2862	96	74	94	95	94	93	96	0.20	0.00	-0.51	-0.47	-0.45	-0.44	-1.08	0.00
TH	2713	99	98	99	99	99	99	99	2708	99	98	98	98	98	99	99	-0.18	-0.22	-0.37	-1.04	-0.98	-0.85	0.00	0.00
TH	2610	99	99	99	99	99	99	99	2613	99	98	99	99	99	99	99	0.11	-0.17	-0.70	-0.27	-0.26	-0.30	0.00	0.00
TH	2595	99	99	99	99	99	99	100	2596	99	98	99	99	99	99	99	0.03	-0.18	-0.99	-0.17	-0.16	-0.26	0.00	-1.01
TH	2603	99	99	99	99	99	99	99	2605	99	98	98	99	99	99	99	0.08	-0.17	-0.84	-0.28	-0.27	-0.33	0.00	0.00
TH	2311	98	97	99	98	101	98	100	2313	98	97	98	98	100	98	100	0.08	0.10	0.04	-0.50	-0.25	-0.57	0.00	0.00
TH	2965	96	82	95	95	95	96	97	2970	95	80	94	95	94	96	96	0.16	-0.34	-1.53	-0.72	-0.68	-0.69	0.00	-1.04
TH	2962	99	97	99	99	100	99	100	2964	99	97	99	99	100	99	100	0.07	-0.08	-0.05	-0.37	-0.35	-0.24	0.00	0.00
TH	2592	99	99	99	99	99	99	99	2593	99	98	99	99	99	99	99	0.07	-0.12	-1.02	0.11	0.10	-0.05	0.00	0.00
TH	3398	99	96	99	99	99	99	99	3415	99	95	99	99	99	99	99	0.52	-0.08	-0.33	-0.14	-0.14	-0.15	0.00	0.00
TH	2745	99	94	98	98	98	99	99	2729	99	93	98	98	98	98	99	-0.58	-0.23	-1.38	0.27	0.25	0.17	-1.02	0.00
LED	2586	93	52	91	90	103	88	104	2616	93	51	91	90	102	88	104	1.13	-0.01	-1.42	-0.28	-0.17	-0.20	0.00	0.00
LED	2721	93	61	91	90	104	88	105	2716	93	59	91	89	104	88	105	-0.20	-0.17	-3.39	-0.44	-0.42	-0.06	0.00	0.00
LED	3035	96	83	95	94	100	92	99	3048	96	82	94	94	99	91	98	0.43	-0.30	-1.02	-0.36	-0.20	-0.73	-1.10	-1.02
LED	3092	96	85	93	92	102	92	101	3117	96	87	93	92	102	92	101	0.78	0.29	2.29	0.02	-0.07	0.25	0.00	0.00
LED	3056	96	86	93	92	102	92	101	3047	96	85	93	92	102	92	101	-0.28	-0.22	-1.02	-0.17	-0.09	-0.21	0.00	0.00
LED	5178	81	37	82	80	99	81	101	5173	81	34	82	80	99	81	101	-0.11	-0.32	-9.72	-0.08	0.09	-0.46	0.00	0.00
LED	3091	88	54	88	87	98	88	99	3087	89	54	88	88	98	88	99	-0.15	0.50	1.00	0.57	0.70	-0.36	0.00	0.00
LED	4905	85	34	83	83	93	84	96	4924	85	33	83	84	93	84	95	0.38	0.07	-2.74	0.17	0.24	-0.32	0.00	-1.05
LED	3053	81	31	81	81	97	81	100	3038	80	30	81	80	97	81	100	-0.47	-0.37	-2.21	-0.50	-0.61	0.15	0.00	0.00
LED	3083	81	31	81	80	97	81	100	3088	80	31	81	80	97	81	100	0.17	-0.34	-0.05	-0.35	-0.37	0.00	0.00	0.00
LED	2866	70	-26	71	72	89	74	92	2857	71	-26	71	72	89	74	92	-0.30	0.06	-0.07	0.02	0.01	-0.05	0.00	0.00
LED	2921	91	55	92	92	98	92	100	2905	91	53	92	92	97	91	100	-0.55	-0.42	-2.26	-0.16	-0.03	-0.58	-1.10	0.00
LED	2874	93	59	94	94	97	93	99	2862	93	59	93	94	97	93	99	-0.41	-0.15	-1.19	-0.21	-0.19	-0.09	0.00	0.00
LED	2950	91	53	91	91	98	91	100	2946	91	53	91	91	99	90	101	-0.13	-0.36	-0.72	-0.45	-0.49	0.37	-1.11	0.99
LED	3398	84	22	84	84	96	85	99	3405	84	22	84	84	96	85	99	0.22	0.08	-0.02	-0.01	-0.05	0.12	0.00	0.00

Finally, in Fig. 16 (a), the approximation response for a spectrum of the Sun is shown. It can be seen that the approximation error is higher, this due to the complexity of the SPD since it is counted in the training phase with a number under examples. However, the Fig. 16 (b) shows the approximation for a TH source where the effectiveness of the proposed model can be observed.

Table 2 shows different types of error to demonstrate the adjustment capacity of the neural network implemented. It shows the Sum of Squablack Errors (SSE), Correlation Coefficient (R-value), Root-Mean-Square Error (RMSE) and Normalized Root-Mean-Square Error. The best adjustment is highlighted in bold and the worst in italic.

Finally, in the Table 3, the value of different color rendering metric is shown, 35 different sources were evaluated, with the measublack value, estimated from the SPD (obtained by the system presented in this work) and the error for each one of them.

4. Conclusions

Accurate measurement of a light source spectrum is central to several lighting applications. Although a traceable standard spectroradiometer is recommended where precision is of the utmost importance, a low-cost, flexible spectrometer with internet connectivity offers new opportunities, especially for smart lighting systems. The CMOS-based spectrometer presented here measures the optical radiation quickly, reliably, and efficiently. An MLP was used to reconstruct the SPD of the light source measublack with 10 bands in the visible spectrum, to an SPD of 81 points. The results show that an MLP of four layers and 25 neurons per hidden layer with sigmoidal activation functions can estimate the SPD with a maximum error of 2%. This spectrometer prototype is an example of the results that can be obtained to improve sensing in lighting systems using a combination of hardware and artificial intelligence.

Conflicts of Interest

None.

Acknowledgments

This study were supported by the Automática, Electrónica y Ciencias Computacionales (AE&CC) Group COL0053581, at the Sistemas de Control y Robótica Laboratory, attached to the Instituto Tecnológico Metropolitano.

References

[1] D. Durmus, W. Davis, Object color naturalness and attractiveness with spectrally optimized illumination, Opt. Express 25 (11) (2017) 12839, doi:10.1364/OE.25.012839.
[2] R.J. Lucas, S.N. Peirson, D.M. Berson, T.M. Brown, H.M. Cooper, C.A. Czeisler, M.G. Figueiro, P.D. Gamlin, S.W. Lockley, J.B. O'Hagan, L.L.A. Price, I. Provencio, D.J. Skene, G.C. Brainard, Measuring and using light in the melanopsin age, Trends Neurosci. 37 (1) (2014) 1–9, doi:10.1016/j.tins.2013.10.004.
[3] P.V. Algvere, J. Marshall, S. Seregard, Age-related maculopathy and the impact of blue light hazard, Acta Ophthalmol. Scand. 84 (1) (2006) 4–15, doi:10.1111/j.1600-0420.2005.00627.x.
[4] P.H. Shaikh, N.B.M. Nor, P. Nallagownden, I. Elamvazuthi, T. Ibrahim, A review on optimized control systems for building energy and comfort management of smart sustainable buildings, Renewable Sustainable Energy Rev. 34 (2014) 409–429, doi:10.1016/j.rser.2014.03.027.
[5] D. Durmus, Optimising Light Source Spectrum to Reduce the Energy Absorbed by Objects, Ph.D. thesis, The University of Sydney, 2015.
[6] D. Durmus, W. Davis, Blur perception and visual clarity in light projection systems, Opt. Express 27 (4) (2019) A216–A223, doi:10.1364/OE.27.00A216.
[7] J.S. Botero-Valencia, F.E. Lopez-Giraldo, J.F. Vargas-Bonilla, Classification of artificial light sources and estimation of Color Rendering Index using RGB sensors, K Nearest Neighbor and Radial Basis Function, Int. J. Smart Sens. Intell. Syst. 8 (3) (2015) 1505–1524, doi:10.21307/ijssis-2017-817.

[8] J.S. Botero-Valencia, F.E. Lopez-Giraldo, J.F. Vargas-Bonilla, Characterization of photodectors using a monochromator and a broadband light source in the XYZ color space, Int. J. Smart Sens. Intell. Syst. 9 (2) (2016) 752–764, doi:10.21307/ijssis-2017-893.

[9] J.S. Botero-Valencia, S. Navarro, N. Giraldo, L. Atehortua, Estimation of photosynthetically active radiation (PAR) using a low cost spectrometer, IEEE Latin Am. Trans. 12 (2) (2014) 107–111, doi:10.1109/TLA.2014.6749525.

[10] D. Pavanello, R. Galleano, R. Kenny, D. Pavanello, R. Galleano, R.P. Kenny, Uncertainty propagation of spectral matching ratios measured using a calibrated spectroradiometer, Appl. Sci. 8 (2) (2018) 186, doi:10.3390/app8020186.

[11] S.W. Brown, Y. Ohno, NIST reference spectroradiometer for color display calibrations, Color Imaging Conf. 1998 (1) (1998) 62–64.

[12] C. DeCusatis, Optical Society of America., Handbook of Applied Photometry, AIP Press, Woodbury N.Y.; Washington DC, 1997.

[13] M. Mansoor, I. Haneef, S. Akhtar, A.D. Luca, F. Udrea, Silicon diode temperature sensors-a review of applications, Sens. Actuators A 232 (2015) 63–74, doi:10.1016/j.sna.2015.04.022.

[14] G.-S. Jeong, W. Bae, D.-K. Jeong, Review of CMOS integrated circuit technologies for high-Speed photo-detection, Sensors 17 (9) (2017) 1962, doi:10.3390/s17091962.

[15] M. Bigas, E. Cabruja, J. Forest, J. Salvi, Review of CMOS image sensors, Microelectron. J. 37 (5) (2006) 433–451, doi:10.1016/j.mejo.2005.07.002.

[16] Avantes 2017 URL http://www.wacolab.com/avantes/spectrometers5.pdf.

[17] THE NATIONAL ACADEMIES PRESS Assessment of Advanced Solid-State Lighting, Washington, 2013. doi:10.17226/18279.

[18] Y. Ohno, Optical metrology for LEDs and solid state lighting, Vol. 6046, International Society for Optics and Photonics, 2006, p. 604625, doi:10.1117/12.674617.

[19] M.P. Royer, Lumen and Chromaticity Maintenance of LED PAR38 Lamps Operated in Steady-State Conditions, Technical Report PNNL-23988, Pacific Northwest National Lab, Richland, WA (United States), 2014.

[20] Y. Ohno, P. Blattner, Chromaticity Difference Specification for Light Sources, Technical Report CIE TN 001:2014, International Commission on Illumination - CIE, 2014.

[21] D.B. Judd, D.L. MacAdam, G. Wyszecki, H.W. Budde, H.R. Condit, S.T. Henderson, J.L. Simonds, Spectral distribution of typical daylight as a function of correlated color temperature, J. Opt. Soc. Am. 54 (8) (1964) 1031, doi:10.1364/JOSA.54.001031.

[22] S. Afshari, S. Mishra, A. Julius, F. Lizarralde, J.D. Wason, J.T. Wen, Modeling and control of color tunable lighting systems, Energy Build. 68 (2014) 242–253, doi:10.1016/j.enbuild.2013.08.036.

[23] F. Dong, A. Sanderson, A dynamic adaptive light field sampling approach for smart lighting control, Light. Res. Technol. 46 (5) (2014) 593–614, doi:10.1177/1477153513502030.

[24] D. Durmus, W. Davis, Optimising light source spectrum for object reflectance, Opt. Express 23 (11) (2015) A456, doi:10.1364/OE.23.00A456.

[25] A. Durmus, D. Abdalla, A. Duis, W. Davis, Spectral optimization to minimize light absorbed by artwork, LEUKOS (2018) 1–10, doi:10.1080/15502724.2018.1533852.

[26] D.M. Berson, F.A. Dunn, M. Takao, Phototransduction by retinal ganglion cells that set the circadian clock, Science 295 (5557) (2002) 1070–1073, doi:10.1126/science.1067262.

[27] S. Hattar, H.-W. Liao, M. Takao, D.M. Berson, K.-W. Yau, Melanopsin-containing retinal ganglion cells: architecture, projections, and intrinsic photosensitivity, Science 295 (5557) (2002) 1065–1070, doi:10.1126/science.1069609.

[28] J. Hye Oh, S. Ji Yang, Y. Rag Do, Healthy, natural, efficient and tunable lighting: four-package white LEDs for optimizing the circadian effect, color quality and vision performance, Light 3 (2) (2014), doi:10.1038/lsa.2014.22. e141–e141

[29] Y.-J. Park, J.-H. Choi, M.-G. Jang, Optimization of light source combination through the illuminance and color temperature simulation of circadian lighting apparatus, J. Korea Contents Assoc. 9 (8) (2009) 248–254, doi:10.5392/JKCA.2009.9.8.248.

[30] P. Elejoste, I. Angulo, A. Perallos, A. Chertudi, I. Zuazola, A. Moreno, L. Azpilicueta, J. Astrain, F. Falcone, J. Villadangos, P. Elejoste, I. Angulo, A. Perallos, A. Chertudi, I.J.G. Zuazola, A. Moreno, L. Azpilicueta, J.J. Astrain, F. Falcone, J. Villadangos, An easy to deploy street light control system based on wireless communication and LED technology, Sensors 13 (5) (2013) 6492–6523, doi:10.3390/s130506492.

[31] K.J. Gaston, T.W. Davies, J. Bennie, J. Hopkins, REVIEW: reducing the ecological consequences of night-time light pollution: options and developments, J. Appl. Ecol. 49 (6) (2012) 1256–1266, doi:10.1111/j.1365-2664.2012.02212.x.

[32] CIE, CIE 157:2004 Control of Damage to Museum Objects by Optical Radiation, Technical Report, Commission Internationale de l'Éclairage, Vienna, Austria, 2004.

[33] Lighting Passport 2018 URL https://www.lightingpassport.com/.

[34] AIBC International 2018 URL http://www.aibcusa.com/portable-led-light-spectrometer.

[35] Allied Scientific Pro 2018 - Spectral Light Meter SRI2000 Illuminance Spectrometer, URL https://alliedscientificpro.com.

[36] F. Rosenblatt, Principles of Neurodynamics: Perceptrons and the theory of Brain Mechanisms, Report (Cornell Aeronautical Laboratory), Spartan Books, 1962.

[37] AMS 2019a URL https://ams.com/as7262.

[38] AMS, 2019b URL https://ams.com/as7263.

[39] CIE, CIE 13.3: Method of Measuring and Specifying Colour Rendering Properties of Light Sources, Technical Report, Commission Internationale de l'Éclairage, Vienna, Austria, 1995.

[40] W. Davis, Y. Ohno, Color quality scale, Opt. Eng. 49 (3) (2010) 033602, doi:10.1117/1.3360335.

[41] I.E. Society, IES Method for Evaluating Light Source Color Rendition, Technical memorandum series, Illuminating Engineering Society of North America, 2015.

[42] CIE, CIE 15: Colorimetry, Technical Report, Commission Internationale de l'Éclairage, Vienna, Austria, 2004.

[43] W. Davis, Y. Ohno, Approaches to color rendering measurement, J. Mod. Opt. 56 (13) (2009) 1412–1419, doi:10.1080/09500340903023733.

[44] W. Xu, M. Wei, K. Smet, Y. Lin, The prediction of perceived colour differences by colour fidelity metrics, Light. Res. Technol. 49 (7) (2017) 805–817, doi:10.1177/1477153516653650.

[45] M. Wei, M. Royer, H.-P. Huang, Perceived color fidelity under LEDs with similar R_f but different R_a, Light. Res. Technol. (2019), doi:10.1177/1477153519825997.

[46] Y. Ohno, Practical use and calculation of CCT and duv, LEUKOS 10 (1) (2014) 47–55, doi:10.1080/15502724.2014.839020.

[47] CIE, CIE TN001: Chromaticity Difference Specification for Light Sources, Technical Report, Commission Internationale de l'Éclairage, Vienna, Austria, 2014.

[48] CIE, CIE 191: Recommended System for Mesopic Photometry Based on Visual Performance, Technical Report, Commission Internationale de l'Éclairage, Vienna, Austria, 2010.

[49] Artificial Neural Network and Supervised Learning, Springer Berlin Heidelberg, Berlin, Heidelberg, 2008 pp. 23–50. doi:10.1007/978-3-540-77481-5_3.

[50] A. Landi, P. Piaggi, M. Laurino, D. Menicucci, Artificial neural networks for nonlinear regression and classification, in: 2010 10th International Conference on Intelligent Systems Design and Applications, 2010, pp. 115–120, doi:10.1109/ISDA.2010.5687280.

[51] M.I. Jordan, C.M. Bishop, Neural networks, Computing Handbook, Third Edition: Computer Science and Software Engineering, 2014. pp. 42: 1–24

[52] Z. Zeng, T. Huang, W.X. Zheng, Multistability of recurrent neural networks with time-varying delays and the piecewise linear activation function, IEEE Trans. Neural Netw. 21 (8) (2010) 1371–1377, doi:10.1109/TNN.2010.2054106.

[53] C.-W. Lin, J.-S. Wang, A digital circuit design of hyperbolic tangent sigmoid function for neural networks, in: 2008 IEEE International Symposium on Circuits and Systems, 2008, pp. 856–859, doi:10.1109/ISCAS.2008.4541553.